MATERIALE PLASTICE
https://revmaterialeplastice.ro
https://doi.org/10.37358/Mat.Plast.1964

Effect of Optimised Infill Parameters on the Tensile Properties of MEX Co-polyester Models

CHEN WANG[1,2]*, JINGYAO LI[1,2], TIANYI WANG[1,2], XIAOWEN WANG[1,2], QING CHU[1,2]
[1] Nanjing Forestry University, College of Furnishings and Industrial Design, Nanjing Jiangsu, China
[2] Jiangsu Co-Innovation Center of Efficient Processing and Utilization of Forest Resources, Jiangsu, China

Abstract: *To optimize the infill parameters and improve the tensile properties of 3D printed polyethylene terephthalate-1,4-cyclohexanedimethanol ester (PETG) models, this study explored the effects of infill thickness, infill flow rate, and infill overlap length on the tensile properties of 3D printed PETG models via the one-way test combined with the Taguchi test. The results of the one-way test showed that the tensile strength and elastic modulus of the PETG models increased with the increase of infill thickness, infill flow rate, and infill overlap length. The results of Taguchi's test showed that the influence of infill parameters on the tensile properties of PETG models was as follows: infill thickness > infill flow rate > infill overlap length; the optimized infill parameters were: infill thickness of 1.2 mm, infill flow rate of 120%, and infill overlap length of 2.8 mm, and the tensile strength of the 3D printed PETG models with optimized parameters was 20.13 MPa, and elastic modulus was 1.32 GPa, which gave the best tensile properties.*

Keywords*: infill parameters, MEX, PETG models, tensile properties*

1. Introduction

Polyethylene terephthalate-1,4-cyclohexanedimethanol ester (PETG) is a non-crystalline co-polyester and a bio-based plastic. It is synthesised from bio-based glycol produced from sugar cane ethylene. This plastic has good light transmission, impact resistance and weather resistance, and it has a short thermoforming cycle and high yield. When 3D printing, PETG material has a low shrinkage rate and almost no odour during the printing process, which makes PETG material has a wide range of application prospects in the field of industrial manufacturing, medical devices and daily necessities, and it is especially suitable for manufacturing products with high requirements for light transmittance, such as transparent plastic plates, cosmetic bottles, and advertisement luminous characters [1-4].

Material extrusion-based additive manufacturing (MEX) is one of the most popular 3D printing processes, featuring a simple printing principle, high processing efficiency, and low equipment cost, etc. MEX uses layer-by-layer stacking to generate solid models. Typically, the interior of PETG models manufactured by MEX is not solid and contains shells and infill structures, which are similar to the structure of plastic shells manufactured by injection moulding process. Among them, the infill structures are equivalent to the strengthening ribs in the injection moulded parts, which play the role of enhancing the structural strength and stiffness of the models [5-8].

Material properties, process parameters and post-processing operations affect the tensile properties of 3D printed PETG models. Infill parameters, as one of the important components of MEX process parameters, have a major impact on the tensile properties of 3D printed PETG models. Infill parameters mainly contain elements such as infill pattern, infill rate, infill thickness, infill flow rate, and infill overlap length. A summary of the relevant literature shows that the existing studies mainly analyse the effects of parameters such as infill pattern and infill rate on the tensile properties of 3D printed PETG models, while fewer studies have been conducted on parameters such as infill thickness, infill flow rate, and infill overlap length [9-11].

In order to improve the tensile properties of 3D printed PETG models, this paper selects infill thickness, infill flow rate, and infill overlap length as the influencing factors, and explores the effects of

email: 996869559@qq.com

infill thickness, infill flow rate, and infill overlap length on the tensile properties of 3D printed PETG models through the one-way test combined with the Taguchi test. It provides a reference for optimising the infill parameters and improving the mechanical properties of PETG models.

2. Materials and methods

2.1. Materials

The PETG filament (White color, 1.75 mm diameter, Miracle 3D, Suzhou, China) was used for additive manufacturing by MEX.

2.2. Specimen preparation

Referring to the 1A dumbbell-type specimen specified in ISO 527.2-2012 standard, the 3D model shown in Figure 1 was designed by Solidworks software (Dassault Systemes, Education Version 2016, Paris, France). The PETG models were printed using a G-450 3D printer (XYZ printing, 0.4 mm nozzle diameter, Miracle 3D, Suzhou, China), and the specific printing parameters were set as follows: nozzle temperature 220^{o}C, hot bed temperature 65^{o}C, layer height 0.2 mm, and printing speed 50 mm/min. In order to minimise the interference of the top and bottom shells of the models on the experimental results, and to highlight the effect of the infill parameters on the tensile properties of the PETG models, the thicknesses of the top and bottom shells were set to 0.4 mm, which means that the top and bottom shells were printed in two layers each [12-14].

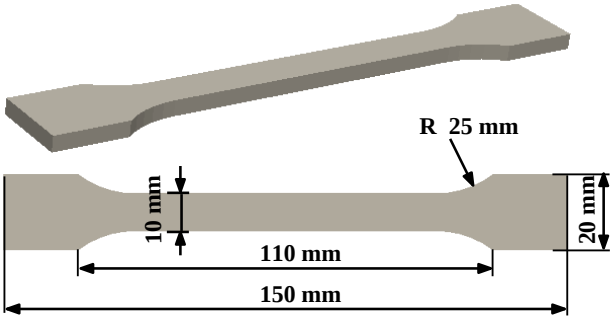

Figure 1. 1A dumbbell-type specimen

2.3. Performance test

A universal mechanical testing machine (AG-X, 20 KN, Shimadzu, Kyoto, Japan) was used to test the tensile properties of groups of PETG models, and the reference standard was ISO 527.2-2012. In addition, the ambient temperature for this test was 20^{o}C, and the loading speed was 2 mm /min. The experimental procedure is shown in Figure 2.

An industrial flush-focus microscope (CL-MA-50M, Colomer, Guangzhou, China) was used to observe the microscopic features of PETG models.

Figure 2. Tensile properties test

3. Results and discussions

3.1. Effect of infill thickness on tensile properties of PETG models

The tensile strength and elastic modulus of PETG models with different infill thicknesses (0.4 mm, 0.8 mm, and 1.2 mm) were tested by setting the infill flow rate of 100% and infill overlap length of 0.04 mm, and the test results of nine groups of PETG models are shown in Figure 3. As seen in Figure 3, the tensile strength and elastic modulus of the PETG models increase as the infill thickness increases. Typically, when the nozzle prints the same infill pattern, a single print can form a single thin-walled infill structure, while multiple prints can form multiple thin-walled infill structures connected side by side, thus effectively increasing the thickness of the infill structures (Figure 4). The infill structures are similar to the strengthening ribs in injection moulded parts. For injection moulded parts, as the thickness of the strengthening ribs increases, the ability of the injection moulded parts to resist damage and deformation from external forces increases [15-17]. Similarly, for 3D printed PETG models, as the thickness of the infill structures increases, the bearing area of any cross-section of the PETG models in the tensile direction increases, which leads to a decrease in the tensile stress per unit area and an increase in the tensile strength and elastic modulus of the PETG models.

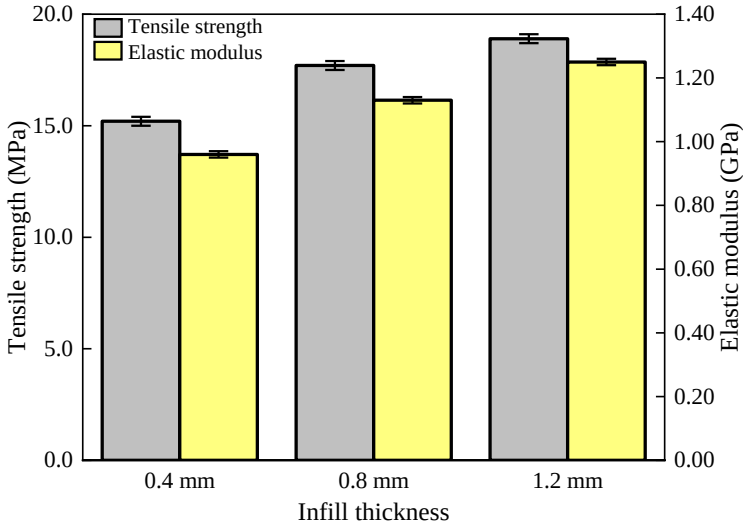

Figure 3. Comparison of tensile strength and elastic modulus

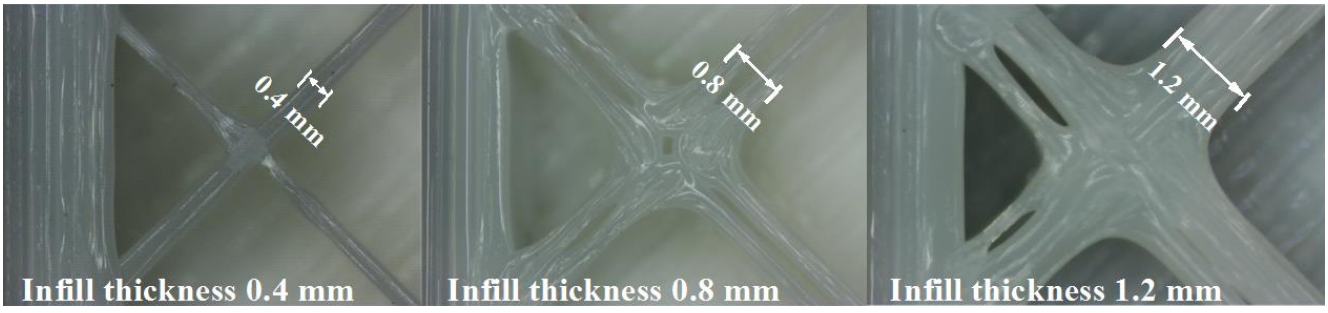

Figure 4. Microscopic comparison of infill thickness

3.2. Effect of infill flow Rate on tensile properties of PETG models

The tensile strength and elastic modulus of PETG models with different infill flow rates (100%, 110%, and 120%) were tested by setting the infill thickness of 0.8 mm and infill overlap length of 0.04 mm, and the test results of nine groups of PETG models are shown in Figure 5. The infill flow rate is the amount of molten filament extruded from the nozzle per unit of time when printing infill structures. Since the molten filament extruded from the nozzle is elliptical in shape, pores are usually present at the combination of the vertical and horizontal filaments, which are prone to stress concentrations and lead

to damage of the model. As the infill flow rate increases, the extruded amount of molten filament material in the nozzle increases, and under the effect of vertical squeezing force in the nozzle, the molten filament material is squeezed and flows at the adhesive interface, which fills the pore defects [18-20]. As can be seen in Figure 6, the pores gradually become smaller as the infill flow rate increases (from 100% to 120%). When the infill flow rate is 120%, the pores are completely filled. And with the disappearance of pores, the PETG models are less likely to be damaged in tension, so their tensile strength and elastic modulus increase.

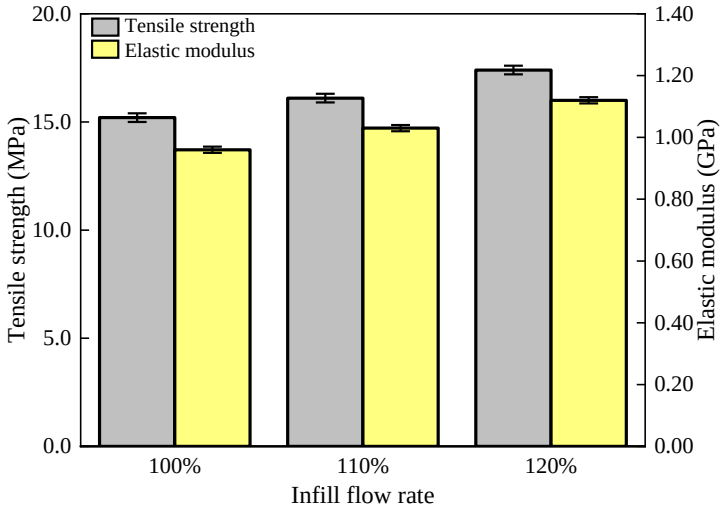

Figure 5. Comparison of tensile strength and elastic modulus

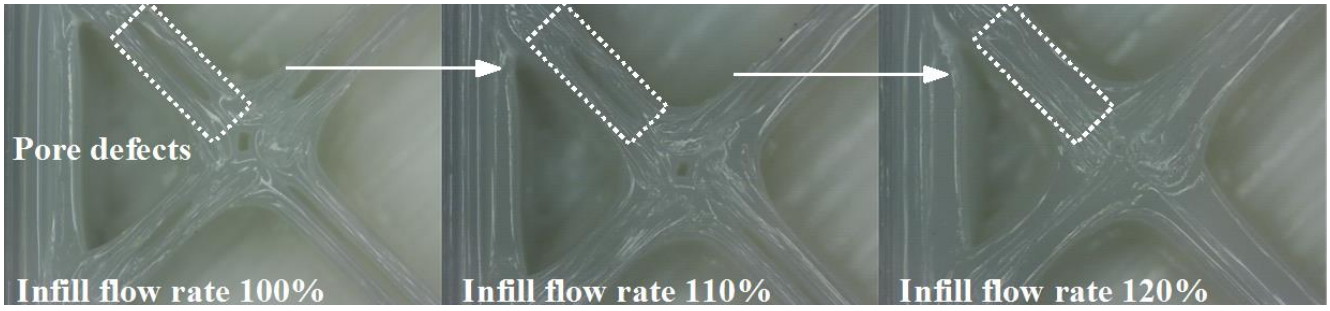

Figure 6. Microscopic comparison of infill flow rate

3.3. Effect of infill overlap length on tensile properties of PETG models

The tensile strength and elastic modulus of PETG models with different infill overlap lengths (0.12 mm, 0.20 mm, 0.28 mm) were tested by setting the infill flow rate of 100% and infill thickness of 0.8 mm, and the test results of nine groups of PETG models are shown in Figure 7. The infill overlap length is the size of the overlap region (connection region) between the infill structure and the sidewall structure in the PETG models. Under the tensile condition, the infill structures and the sidewall structures carry the load together and resist the damage and deformation of the external force together. As the overlap length increases, the volume of the overlap region between the infill structures and the sidewall structures increases (Figure 8), and the number of crosslinked polymer molecules in the overlap region increases. Under the same loading conditions, the tensile stress can be more uniformly dispersed in the infill and sidewall structures, which makes the integrity and load-bearing performance of the PETG models stronger, so their tensile strength and elastic modulus increase.

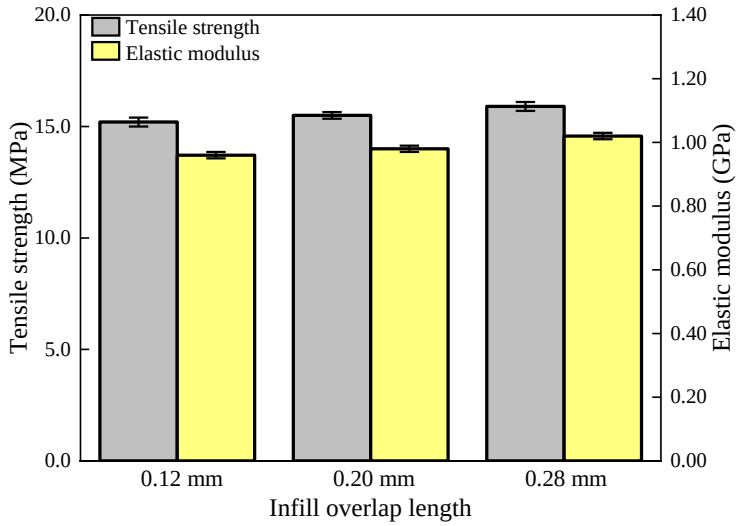

Figure 7. Comparison of tensile strength and elastic modulus

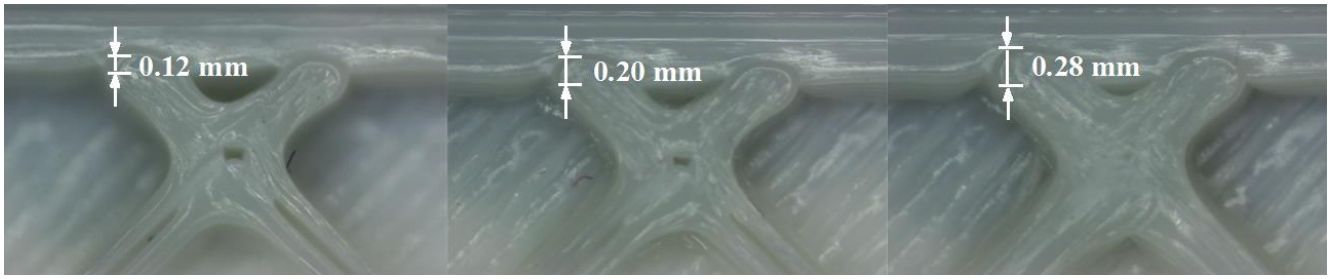

Figure 8. Microscopic comparison of infill overlap length

3.4. Taguchi test

3.4.1. Design of the Taguchi Test

In order to optimise the infill parameters and further improve the tensile properties of 3D printed PETG models. Infill thickness, infill flow rate, and infill overlap length were selected as the influencing factors to be analysed in Taguchi test, and three levels were set for each factor (Table 1) to produce the L9-type orthogonal test table.

Table 1. Factor level table

Levels	Influencing factors		
	Infill thickness (*A*)/mm	**Infill flow rate (*B*)/mm**	**Infill overlap length (*C*)/mm**
1	0.4	100%	0.12
2	0.8	110%	0.20
3	1.2	120%	0.28

3.4.2. Signal-to-noise ratio analysis

The Taguchi test data (Table 2) were calculated and analysed. The research objective of this paper is to improve the tensile properties of 3D printed PETG models, so the data were analysed using "larger-the-better" quality characteristic, the calculation formula is: $S/N = -10\lg\left(\frac{1}{N}\sum\frac{1}{T_i^2}\right)$. The nine groups of tensile strength and elastic modulus data obtained from orthogonal tests were weighted and summed, and the tensile properties weighted value T_i was obtained by normalising the tensile strength and elastic modulus with linear functions and setting the weighting coefficients to 0.5 for each of them. The Taguchi test was analysed for nine sets of weighted values of tensile properties T_i, and a signal-to-noise response

table (Table 3) and a signal-to-noise response graph (Figure 9) were obtained for the tensile properties of the PETG models.

Table 2. Orthogonal test table

Serial number	Infill thickness (mm)	Infill flow rate	Infill overlap length (mm)	Tensile strength (MPa)	Elastic modulus (GPa)	weighted value T_i
1	A_1 (0.4)	B_1 (100%)	C_1 (0.12)	15.21	0.96	0.7667
2	A_1 (0.4)	B_2 (110%)	C_2 (0.20)	15.50	0.98	0.7821
3	A_1 (0.4)	B_3 (120%)	C_3 (0.28)	15.92	1.02	0.8085
4	A_2 (0.8)	B_1 (100%)	C_2 (0.20)	17.81	1.13	0.9002
5	A_2 (0.8)	B_2 (110%)	C_3 (0.28)	18.23	1.16	0.9227
6	A_2 (0.8)	B_3 (120%)	C_1 (0.12)	18.01	1.17	0.9209
7	A_3 (1.2)	B_1 (100%)	C_3 (0.28)	18.90	1.25	0.9751
8	A_3 (1.2)	B_2 (110%)	C_1 (0.12)	19.34	1.27	0.9943
9	A_3 (1.2)	B_3 (120%)	C_2 (0.20)	19.41	1.28	1.0000

Table 3. Signal-to-noise ratio response table

Levels	Influencing factors		
	Infill thickness (*A*)/mm	Infill flow rate (*B*)/mm	Infill overlap length (*C*)/mm
1	-2.0962	-1.1465	-1.0243
2	-0.7759	-0.9616	-1.0159
3	-0.0895	-0.8540	-0.9214
S/N	2.0066	0.2925	0.1029
sorting	1	2	3

From Table 3, it can be seen that factor *A* (infill thickness) has the largest rank value of 2.0066, which has the greatest impact on the tensile properties of the PETG models; The rank value of factor *B* (infill flow rate) is in the middle, with a value of 0.2925, and its impact on the tensile properties of the PETG models is secondary; The rank value of factor *C* (infill overlap length) is the smallest, with a value of 0.1029, which has the smallest impact on the tensile properties of the PETG models. The signal-to-noise response graph further validates the above conclusion, as seen in Figure 9, the slope of the infill thickness response curve is the largest, the slope of the infill flow response curve is secondary, and the slope of the infill overlap length response curve is the smallest.

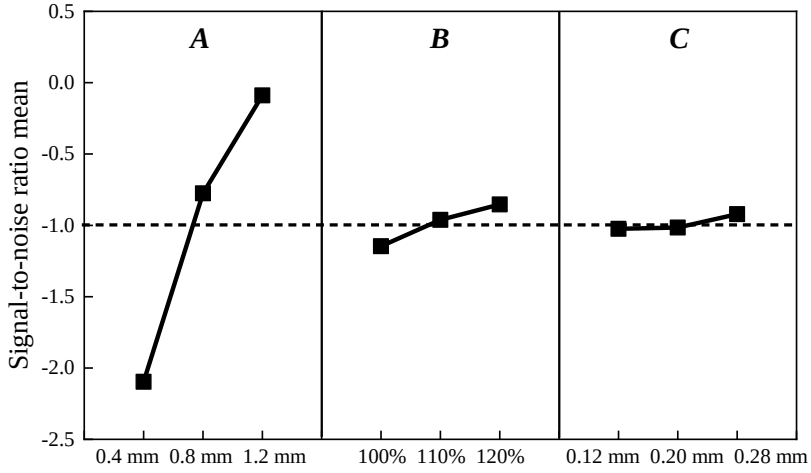

Figure 9. Signal-to-noise ratio response graph

In summary, the optimal combination of tensile parameters is $A_3B_3C_3$, i.e., infill thickness of 1.2 mm, infill flow rate of 120%, and infill overlap length of 2.8 mm. To validate the test results, PETG models were produced using an MEX printer according to the parameters corresponding to this optimal combination, and tensile properties tests were conducted on the PETG models, which resulted

in a tensile strength of 20.13 MPa and a elastic modulus of 1.32 GPa, both of which were higher than the maximum values of tensile strength and elastic modulus in the orthogonal test design table. To further verify the reliability of the results, the models were fabricated using an Anycuble Kobra (desktop grade) fused deposition 3D printer with the same combination of parameters, and the tensile strength of the models was measured to be 20.25 MPa and the elastic modulus to be 1.33 GPa, which verified that $A_3B_3C_3$ was the optimal solution.

4. Conclusions

To investigate the effects of infill thickness, infill flow rate, and infill overlap length on the tensile properties of 3D printed PETG models. A one-way test analysis showed that the tensile strength and elastic modulus of PETG models increased with the increase of infill thickness, infill flow rate, and infill overlap length.

Infill thickness, infill flow rate and infill overlap length were selected as the influencing factors, and the analysis of Taguchi's test showed that: the degree of influence of infill parameters on the tensile properties of PETG models is: infill thickness > infill flow rate > infill overlap length; the optimised infill parameters are: infill thickness 1.2 mm, infill flow rate 120%, infill overlap length 2.8 mm; under these optimised parameters, the 3D printed PETG models have a tensile strength of 20.13 MPa and a elastic modulus of 1.32 GPa, which is the best tensile properties.

References

1. FENG, X. H., WU, Z. H., SANG, R. J., WANG, F., ZHU, Y. Y., WU, M. J., Surface design of wood-based board to imitate wood texture using 3D printing technology, *BioResources*, 2019, 14(4), 8196-8211.
2. DING, T. T., YAN, X. X., ZHAO, W. T., Effect of urea-formaldehyde resin-coated colour-change powder microcapsules on performance of waterborne coatings for wood surfaces, *Coatings*, 2022, 12(9), 1289.
3. FENG, X. H., YANG, Z. Z., WANG, S. Q., WU, Z. H., The reinforcing effect of lignin-containing cellulose nanofibrils in the methacrylate composites produced by stereolithography, *Polymer Engineering and Science*, 2022(9), 2968-2976.
4. HAN, Y., YAN, X. X., ZHAO, W. T., Effect of thermochromic and photochromic microcapsules on the surface coating properties for metal substrates, *Coatings*, 2022, 12(11), article 1642.
5. LI, R. R., CHEN, J. J., WANG, X.-D., Prediction of the color variation of moso bamboo during CO2 laser thermal modification, *BioResources*, 2020, 15(3), 5049-5057.
6. LIU, Q., GU, Y., XU, W., LU, T., LI, W., FAN, H., Compressive properties of green velvet material used in mattress bedding, *Applied Sciences*, 2021, 11(23), article 11159.
7. LI, W. B., YAN, X. X., ZHAO, W. T., Preparation of crystal violet lactone complex and its effect on discoloration of metal surface coating, *Polymers*, 2022, 14(20), 4443.
8. HUANG, N., YAN, X. X., ZHAO, W. T., Influence of photochromic microcapsules on properties of waterborne coating on wood and metal substrates, *Coatings*, 2022, 12(11), article 1750.
9. LIU, X. Y., LV, M. Q., LIU, M., LV, J. F., Repeated humidity cycling's effect on physical properties of three kinds of wood-based panels, *BioResources*, 2019, 14(4), 9444-9453.
10. WANG, X. H., WU, Y., CHEN, H., ZHOU, X. Y., ZHANG, Z. K., XU, W., Effect of surface carbonization on mechanical properties of LVL, *BioResources*, 2019, 14(1), 453-463.
11. ZHOU, C. M., HUANG, T., LUO, X., KANER, Jake., Reorganisation and construction of an age-friendly smart recreational home system: based on function-capability match methodology, *Applied Sciences-Basel*, 2023, 13(7), 9783.
12. QI, Y. Q., SUN, Y., ZHOU, Z. W., HUANG, Y., LI, J. X, LIU, G. Y., Response surface optimization based on freeze-thaw cycle pretreatment of poplar wood dyeing effect, *Wood Research*, 2023, 68(2), 293-305.

13. LIU, Y., HU, J., WU, Z. H., Fabrication of coatings with structural color on a wood surface, *Coatings*, 2020, 10(1), article 32.
14. WANG, L., HAN, Y., YAN, X. X., Effects of adding methods of fluorane microcapsules and shellac resin microcapsules on the preparation and properties of bifunctional waterborne coatings for basswood, *Polymers*, 2022, 14(18), 3919.
15. YANG, L., HAN, T. Q., LIU, Y. X., Yin, Q., Effects of vacuum heat treatment and wax impregnation on the color of pterocarpus macrocarpus kurz, *BioResources*, 2021, 16(1), 954-963.
16. WANG, Q., FENG, X. H., LIU, X. Y., Functionalization of nanocellulose using atom transfer radical polymerization and applications: A review, *Cellulose*, 2023, 30, 8495-8537.
17. YANG, Z. Z., FENG, X. H., XU, M., RODRIGUE, D., Printability and properties of 3D printed poplar fiber/polylactic acid biocomposites, *BioResources*, 2022, 16(2), 2774-2788.
18. ZHOU, C. M., HUANG, T., LIANG, S., Smart home R&D system based on virtual reality, *Journal of Intelligent & Fuzzy Systems*, 2020, 40(2), 3045–3054.
19. MO, X. F., ZHANG, X. H., FANG, L., ZHANG, Y., Research progress of wood-based panels made of thermoplastics as wood adhesives, *Polymers*, 2022, 14(1), article 98.
20. ZHOU, J. C., XU, W., Toward interface optimization of transparent wood with wood color and texture by silane coupling agent. *Journal of Materials Science*, 2022, 57(10), 5825-5838.

Manuscript received: 4.04.2024